Near-Field Infrared Sum-Frequency Generation Imaging of Chemical Vapor Deposited Zinc Selenide

Richard D. Schaller and Richard J. Saykally*

Department of Chemistry, University of California, Berkeley, California 94720-1460

Received October 26, 2000. In Final Form: January 10, 2001

Infrared sum-frequency generation (SFG) has been detected with near-field scanning optical microscopy (NSOM) for the first time. SFG NSOM images of a chemical vapor deposited (CVD) disk of zinc selenide were recorded as a function of infrared (IR) wavelengths ranging from 3.1 to 4.4 μm from an amplified femtosecond laser. Striation patterns, which are not observed in the topography, were detected in the optical images and exhibited increased SFG in comparison to homogeneous regions of the semiconductor. SFG images were demonstrated to have $\sim \lambda/20$ spatial resolution in comparison to the IR wavelengths used to produce the sum frequency.

Introduction

Sum-frequency generation (SFG) spectroscopy is a well-established optical technique for the study of surfaces and interfaces that is applicable to a wide range of samples.[1−5] Generally, SFG experiments involve overlapping a fixed-frequency visible or near-IR (pump) pulse in space and time with a tunable IR pulse on a sample. The second-order nonlinear susceptibility of the sample ($\chi^{(2)}$) couples the electric fields and produces a radiating polarization ($P^{(2)}$) at the SF according to the equation

$$P^{(2)}(\omega_{SF} = \omega_P + \omega_{IR}) \approx \chi^{(2)}_{ijk} E(\omega_P)\, E(\omega_{IR}) \qquad (1)$$

where i, j, and k are laboratory coordinates. $\chi^{(2)}$ consists of a resonant and nonresonant term

$$\chi^{(2)} = \chi^{(2)}_R + \chi^{(2)}_{NR} \qquad (2)$$

Within the dipole approximation, $\chi^{(2)}_R$ can be described by

$$\chi^{(2)}_R \approx \sum_{n,n' \neq g} \frac{\langle g|i|n\rangle}{(\omega_{SF} - \omega_{ng} + i\Gamma_{ng})} \times \left(\frac{\langle n|j|n'\rangle\langle n'|k|g\rangle}{(\omega_P - \omega_{n'g} + i\Gamma_{n'g})} + \frac{\langle n|k|n'\rangle\langle n'|j|g\rangle}{(\omega_{IR} - \omega_{n'g} + i\Gamma_{n'g})} \right) \qquad (3)$$

where ω_{ng} is a molecular transition frequency between the ground state, g, and an excited state, n, and Γ_{ng} indicates the transition's upper state lifetime. A large increase (up to 10^4) in SFG signals may be observed when an optical frequency approaches that of a Raman and dipole active transition.[1] Under the condition that only the IR frequency is resonantly enhanced, the SFG signals allow vibrational analysis of the sample.

Surprisingly, SFG has only recently been demonstrated as a far-field microscopy technique.[6] Due to the phase-matching condition,[1] SFG microscopy signals change laboratory direction as the IR frequency is scanned. This inherent far-field constraint makes imaging with a single alignment difficult. An even more significant problem arises from the spatial resolution that is desired in SFG imaging. Far-field SFG microscopy resolution is determined by the region of spatial overlap of the pump and IR pulses. Thus, the spatial resolution is restricted by the diffraction limit to $\sim\lambda_{pump}/2$.

Detection of SFG with near-field scanning optical microscopy (NSOM) transcends both of these difficulties. Phase-matching conditions are relaxed for near-field detection by an NSOM probe which collects the SF optical field at subwavelength distances from the sample.[7,8] Accordingly, the spatial resolution of SFG NSOM is independent of the pump and IR spot sizes at the sample. Instead, the physical dimensions of the NSOM probe, which can be more than 2 orders of magnitude smaller than far-field spot sizes, determine the spatial localization of the collected optical signal. Moreover, NSOM simultaneously produces a topographical map of the sample surface, similar to atomic force microscope images, which can be used to directly correlate physical sample features with the chemical information contained in the SFG signal. This information is clearly not available with far-field experiments.

Nonlinear optical NSOM techniques are evolving rapidly.[9−14] Second-harmonic generation (SHG) NSOM has been used to investigate membrane-bound organelles,[15] a Langmuir−Blodgett film,[16] metal surfaces,[17] and nanocomposites.[18] Third-harmonic generation NSOM

* Corresponding author. E-mail address: saykally@cchem.berkeley.edu.

(1) Shen, Y. R. *Pricnciples of Nonlinear Optics;* Wiley: New York, 1984.
(2) Bloembergen, N. *Appl. Phys. B* **1999**, *B68*, 289.
(3) Shen, Y. R. *Nature* **1989**, *337*, 519−24.
(4) Boyd, R. *Nonlinear Optics*; Academic: New York, 1992.
(5) McGilp, J. F. *J. Phys. D* **1996**, *29*, 1812.
(6) Florsheimer, M.; Brillert, C.; Fuchs, H. *Langmuir* **1999**, *15*, 5437.
(7) Vigoureux, J. M.; Girard, C.; Depasse, F. *J. Mod. Opt.* **1994**, *41*, 49.
(8) Zhao, X.; Kopelman, R. *Ultramicroscopy* **1995**, *61*, 69.
(9) Smolyaninov, I. I.; Zayats, A. V.; Davis, C. C. *Opt. Lett.* **1997**, *22*, 1592.
(10) Smolyaninov, I. I.; Lee, C. H.; Davis, C. C. *Appl. Phys. Lett.* **1999**, *74*, 1942.
(11) Sanchez, E. J.; Novotny, L.; Xie, X. S. *Phys. Rev. Lett.* **1999**, *82*, 4014.
(12) Bozhevolnyi, S. I.; Vohnsen, B.; Pederson, K. *Opt. Commun.* **1998**, *150*, 49.
(13) Jenei, A.; Kirsch, A. K.; Subramaniam, V.; Arndt-Jovin, D. J.; Jovin, T. M. *Biophys. J.* **1999**, *76*, 1092.
(14) Kirsch, A. K.; Subramaniam, V.; Striker, G.; Schnetter, C.; Amdt-Jovin, D. J.; Jovin, T. M. *Biophys. J.* **1998**, *75*, 1513.
(15) Schaller, R. D.; Roth, C.; Raulet, D. H.; Saykally, R. J. *J. Phys. Chem. B* **2000**, *104*, 5217.
(16) Bozhevolnyi, S. I.; Geisler, T. *J. Opt. Soc. Am. A* **1998**, *15*, 2156.
(17) Smolyaninov, I. I.; Zayats, A. V.; Davis, C. C. *Phys. Rev. B* **1997**, *56*, 9290.
(18) Jakubczyk, D.; Shen, Y.; Lal, M.; Friend, C.; Kim, K. S.; Swiatkiewicz, J.; Prasad, P. N. *Opt. Lett.* **1999**, *24*, 1151.

10.1021/la001513m CCC: $20.00
Published on Web 02/28/2001

has also recently been demonstrated on human erythrocytes.[19] Linear IR near-field microscopy techniques are currently being explored by several groups[20−23] seeking to exploit the powerful chemical signature of vibrational spectra for high spatial resolution imaging. The major difference in these approaches, as compared with SFG NSOM imaging, is that the latter can be surface (interface) specific. This surface selectivity arises from the constraint that, in the dipole approximation, only materials which lack inversion symmetry can produce SF signals, and interfaces necessarily satisfy this condition, whereas the bulk may not. SFG imaging can also yield higher optical contrast than linear IR NSOM because the resonance enhancements can be so large (up to 10^4).[1]

A final issue concerns the spatial resolution differences between linear IR NSOM and SFG NSOM, which again involve the linear scaling of wavelength with the diffraction limit. As the probe tip radius, r, becomes much smaller than λ, the coupling efficiency of the light to the tip is thought to decrease according to $(r/\lambda)^6$.[24] This ratio will be much smaller for IR wavelengths than for visible SFG wavelengths, given a fixed value of r. Because SF signals contain low frequency information, but are detected at visible wavelengths, a large coupling efficiency for the same ultimate IR spatial resolution should also significantly favor the SFG technique.

In this study, we investigated the spatial distribution of SFG intensities from CVD ZnSe, a wide band gap semiconductor (2.8 eV at 300 K) and a strong candidate for use as a blue diode laser.[25,26] Blue diode lasers may be used as an efficient pump source for many other laser materials and as a tool for lithography and high-density optical data processing. Imperfections, impurities, and defects in the semiconductor are believed to reduce the quantum efficiency of the conversion of carriers to emitted photons and present a barrier to potential applications.[27] The characterization of defects in ZnSe is an important effort for the development of functioning blue laser diodes.

Experimental Section

A previously described NSOM system, equipped with a shear-force feedback mechanism, was employed for near-field measurements of SFG signals.[15] Fiber optic probes were adiabatically pulled to a ∼50 nm diameter tip and were not metal coated so as to avoid significant perturbation of the sample.[17] Topographical and optical signals were obtained simultaneously for comparison. The sample was not scanned in a raster pattern, but instead the forward and reverse motions of the sample were collected to produce separate images as a check of reproducibility. Repeatable optical images were then added together to reduce random noise.

The light source for the experiments consisted of a home-built titanium:sapphire oscillator (800 nm, 480 mW, 30 fs, 88 MHz) which was used to seed a commercial (Spectra-Physics) chirped pulse amplifier (800 nm, 2.25 W, 80 fs, 1 kHz). This output was beamsplit 90:10 using 90% to pump a commercial (Quantronix, Topaz) superfluorescence optical parametric amplifier (OPA) (1.16−2.7 μm, 300 μJ at 1350 nm, 80 fs). Tunable mid-IR wavelengths were produced via difference frequency generation between the signal and idler OPA wavelengths in a AgGaS crystal (2.8−10 μm, 20 μJ at 4.4 μm, 155 fs) and mixed on the sample with the residual 10% of the amplifier output (further attenuated to ∼3 μJ).

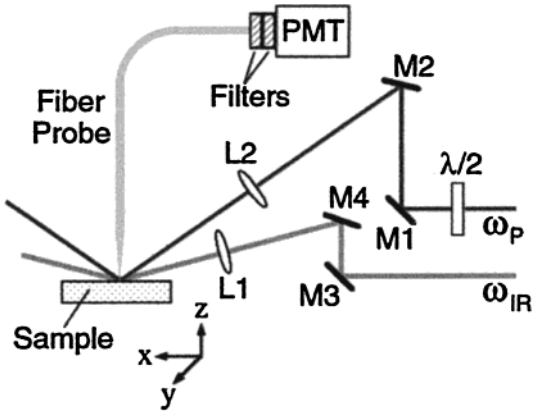

Figure 1. Experimental setup: steering mirrors (M1−4); 8 cm focal length CaF_2 lens (L1); 15 cm focal length fused silica lens (L2). The generated SFG signals were collected by the NSOM fiber probe and directed to two broad band-pass filters centered at 670 nm before measurement by a Hamamatsu 3896 photomultiplier tube (PMT) biased at −1100 V and fast gated electronics. Sample stage piezos perform the x, y, and z directions of motion for both scanning and near-field feedback so that the NSOM probe experiences an invariant tip/field geometry. The tip to sample distance was maintained at ∼5 nm. All images are 200 pixel × 200 pixel x, y arrays, and each pixel represents a (50 nm)^2 area.

As shown in Figure 1, the 800 nm pulse train was incident on the sample at 45° from normal and was focused to a ∼(200 μm)^2 spot for simplicity of alignment. The polarization of the 800 nm light was controlled with a zero order half-waveplate and checked with a polarizing cube. The p-polarized IR pulses were focused on the sample at a 60° angle to a ∼(100 μm)^2 spot size. The overlap of the two spots was spatially coincident with the point at which the NSOM probe investigated the sample. To overlap the pulses in time, the 800 nm pulses were directed through a manually controlled delay line. Typically, 0−5 SFG photons were detected per laser shot and complete images required ∼30 min to collect.

A mechanically polished, 1 mm thick CVD sample of ZnSe (∼100 μm grain size) was washed extensively with methanol and dried under vacuum. As ZnSe lacks centrosymmetry, the presented nonlinear optical studies may have a bulk contribution. However, the images will have a shallow depth of field (sub-wavelength) due to the evanescent wave coupling of signals into the probe which is believed to decay exponentially with distance.[24]

Results and Discussion

Shown in Figure 2, parts **a**−**d**, are SFG NSOM images of the CVD sample of ZnSe for the same (10 μm)^2 topographical area shown in **e**. Images collected with an IR wavelength of 3.3 μm and s- or p-polarized 800 nm light are shown in parts **a** and **b**, respectively, while parts **c** and **d** show images generated with an IR wavelength of 3.8 μm. All of the images exhibited very good reproducibility on forward and reverse scans, and displayed images have not been processed.

Comparison of the topographical and SFG images demonstrates that quite distinct information is obtained with the two imaging techniques. While the physical topography of the surface shows small circular features, ranging in size from 260 to 1800 nm in diameter, each of the SFG images reveals long (700−4300 nm), thin (∼250 nm fwhm) features that are highly parallel to each other. Such features were not observed in other imaged adjacent regions (10 μm away) of the sample using the exact same

(19) Schaller, R. D.; Johnson, J. C.; Saykally, R. J. *Anal. Chem.* **2000**, *72*, 5361.
(20) Dragnea, B.; Preusser, J.; Schade, W.; Leone, S. R.; Hinsberg, W. D. *J. Appl. Phys.* **1999**, *86*, 2795.
(21) Knoll, B.; Keilmann, F. *Nature* **1999**, *399*, 134.
(22) Hong, M. K.; Jeung, A. G.; Dokholyan, N. V.; Smith, T. I.; Schwettman, H. A.; Huie, P.; Erramilli, S. *Nucl. Instrum. Methods Phys. Res. B* **1998**, *144*, 246.
(23) Piednoir, A.; Licoppe, C.; Creuzet, F. *Opt. Commun.* **1996**, *129*, 414.
(24) Paesler, M. A.; Moyer, P. J. *Near-field Optics: Theory, Instrumentation, and Applications*; Wiley: New York, 1996.
(25) Okuyama, H.; Kato, E.; Itoh, S.; Nakayama, N.; Ohata, T.; Ishibashi, A. *Appl. Phys. Lett.* **1995**, *66*, 656.
(26) Park, R. M. *Proc. SPIE−Int. Soc. Opt. Eng.* **1995**, *2524*, 142.
(27) Allen, J. W. *Semicond. Sci. Technol.* **1995**, *10*, 1049.

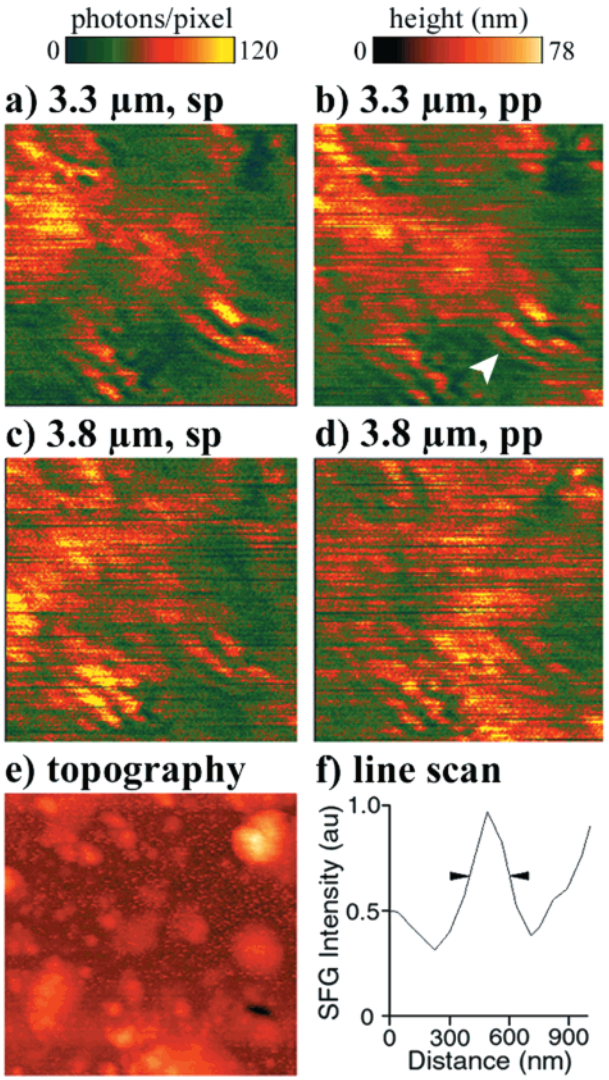

Figure 2. SFG NSOM images of CVD ZnSe. A−d, SFG images of a $(10\,\mu m)^2$ area of ZnSe produced using 800 nm and IR pulses that correspond to the indicated wavelengths and polarization combinations for the same topographical area shown in part e. Readily discernible in the SFG NSOM images, but not observable in the topographical image, are parallel features which are interpreted to be strain patterns within the ZnSe crystal lattice. The striations are thought to form in regions of high impurity concentration.[30] The spatial variation of the optical signals is also clearly observed to vary when the 800 nm light polarization is rotated and/or the IR wavelength is changed. The small white arrow drawn in part b indicates the 111 crystal direction (based on the work of Hocker et al.[30]) as well as the region shown in part f used to determine the spatial resolution of the experimental method. The fwhm of the striation feature shown in part f is indicated and measured to be ∼190 nm, which may be sample limited. Dark areas in the SFG optical images correspond to low signal (∼0 to 1 photons/shot), and bright areas correspond to high signals (∼5 photons/shot). Optical image pixel *z*-values represent the average of 40 laser shots.

laser alignments to the NSOM probe, which precludes the possibility of the striations originating from far-field diffraction artifacts.[29] Striations in polycrystalline ZnSe have also been observed in previous far-field work by Hocker et al. using linear polarized light microscopy, although these observations were on a length scale that was 2 orders of magnitude larger.[30] It was alleged that these striations, which were observed to grow perpendicularly to the 111 crystal axis, may result from regions of strain in the crystal lattice due to increased impurity concentrations in these regions. It was also hypothesized that these strained regions could produce enhancements in SHG signals, although this was not directly investigated in that work. The SFG images in Figure 2 confirm that these regions of strain and possible impurity do in fact produce significant enhancements in the second-order nonlinear response. It appears that enhancement of the SFG signals in these defect regions approaches an order of magnitude when compared to nonstriated areas of the sample.

A line scan of one of the spatially smaller striation features contained in Figure 2**b** is shown in Figure 2**f**. Analysis of the fwhm of this feature shows that the resolution of the SFG NSOM technique can indeed provide very high spatial resolution, here observed to be ∼190 nm. In comparison to the detected sum frequency wavelength, this is a resolution of approximately $\sim\lambda/4$. However, when the consideration is made that the sum frequency contains information related to the IR wavelength involved, a significantly higher effective resolution of $\sim\lambda/20$ for the IR photons has been achieved. Additionally, the high resolution of the images, in particular of the striations, indicates that a shallow depth of field is being realized in the SFG NSOM images because signals generated far away from the surface would be observable over a larger spatial extent.

Variation of the incident polarization of the 800 nm light produces distinct image contrast for the same region of the ZnSe (comparison of **a** to **b** and **c** to **d**). Of the 27 elements of the third rank tensor that describe the bulk second-order response of a material with zinc blende structure, only one nonzero component exists which is 6-fold degenerate: $\chi^{(2)}_{xyz} = \chi^{(2)}_{xzy} = \chi^{(2)}_{yxz} = \chi^{(2)}_{yzx} = \chi^{(2)}_{zxy} = \chi^{(2)}_{zyx}$.[31] For this reason it appears that an additional element of anisotropy is observed in the polarization studies which could have three likely origins: (1) interfacial components of the $\chi^{(2)}$ response which will change dramatically as the symmetry of the crystal lattice breaks down at an interface, (2) resonantly enhanced SFG due to adsorbates, the most likely being water, or (3) resonantly enhanced SFG due to surface states and impurities (traps) present in the semiconductor.[27,28] Nonresonant SFG should remain invariant with small changes in the optical frequencies. The variation in contrast between parts **a** and **c** as well as **b** and **d** of Figure 2 wherein the IR wavelength is changed, thus, is indicative of a resonance enhancement mechanism. Figure 3 illustrates the variation in SFG signals observed when the IR wavelength is tuned from 3.1 to 4.4 μm and exhibits maximum enhancements at $\lambda_{IR} = 3.5\ \mu$m as well as polarization dependence; however, further work is required to characterize the exact nature of this enhancement.

Finally, to confirm that the optical signals in this study do indeed result from the SFG process, an SFG NSOM cross-correlation measurement is shown in Figure 4. The cross-correlation establishes that the measured signal is

(28) Queisser, H. J.; Haller, E. E. *Science* **1998**, *281*, 945.
(29) To further demonstrate that the observed striation patterns did not result from diffraction artifacts, images of the same area shown in Figure 2 were produced with the lasers at slightly varied angles of incidence and resulted in indistinguishable images (not shown). This further indicates that the striation features result from properties of the sample rather than from diffraction artifacts which would change appreciably with even minor laser alignment changes.
(30) Hocker, L. O.; Dewey, C. F. *Appl. Phys. Lett.* **1976**, *28*, 267.
(31) Yamada, C.; Kimura, T. *Phys. Rev. B* **1994**, *49*, 14372.
(32) Schade, W.; Osborn, D. L.; Preusser, J.; Leone, S. R. *Opt. Commun.* **1998**, *150*, 27.
(33) Peng, W. J.; Wang, H.; Wong, K. S.; Wong, G. K. L. *QELS* **1996**, *10*, 55.

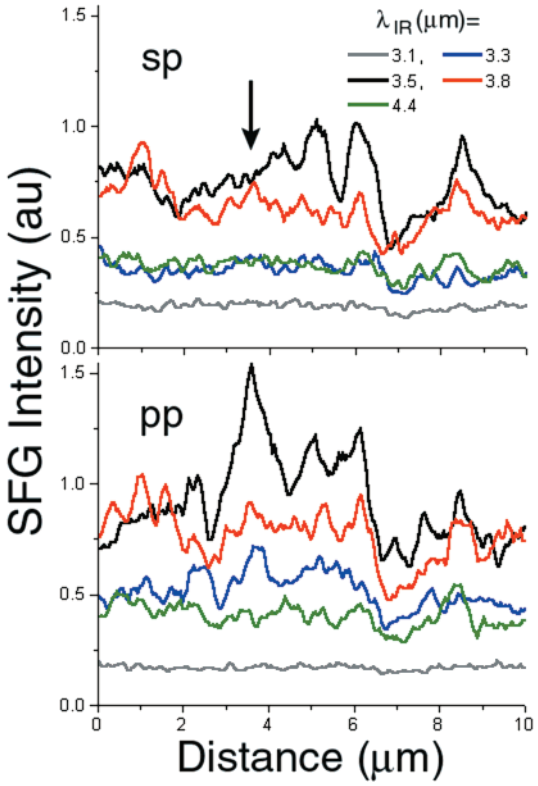

Figure 3. Resonance enhancement in SFG NSOM. Line scans of the same region (10 μm × 50 nm) of the ZnSe were collected using IR wavelengths of equal intensity at 3.1−4.4 μm with the indicated input polarizations (800 nm, IR). The recorded SFG intensities represent the average of 175 laser shots/pixel. This measurement further demonstrates that resonant enhancement is operative in these measurements. SFG signals become strongest when $\lambda_{IR} = 3.5$ μm and become much weaker at 3.1 μm. The black arrow in the figure points to a striation feature that exhibits high input polarization-dependence whereas other striation features appear less sensitive.

only present when the 800 nm and IR photons are temporally overlapped. Deconvolution of the cross-correlation also closely reproduces far-field measurements of the IR pulse width (~155 fs).

The SFG NSOM technique described here for the first time is clearly a very useful new tool for surface imaging. The vibrational spectroscopic information and surface selective properties of SFG, which have been applied to many far-field research problems, will be even more useful when coupled with the high spatial resolution and topographic information that is simultaneously obtainable with NSOM.

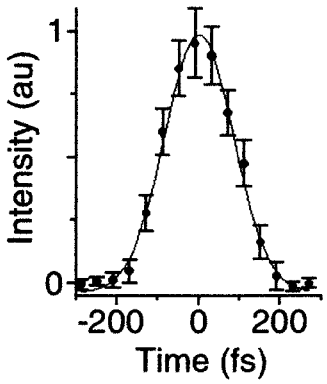

Figure 4. SFG NSOM cross-correlation. The cross-correlation of the SFG signal was produced by varying the temporal delay between the two pulses and recording the signal through the NSOM probe. This measurement demonstrates that the observed signals were only produced when both the pump and IR pulses were temporally overlapped. Each point represents the average of 15 000 laser shots, and rms noise values are displayed. A Gaussian fit to the correlation signal resulted in a fwhm of 185 fs which can be deconvoluted using the formula[32] $\Delta\tau_{cc}(\text{fwhm}) = (\Delta t_{800}^2 + \Delta t_{IR}^2)^{1/2}$. The known value of $\Delta t_{800} = 80$ fs from frequency-resolved optical gating measurements gives ~167 fs as the value for Δt_{IR}, which is consistent with the far-field measurement of ~155 fs. Background light produced via two-photon photoluminescence (which would occur at 450−490 nm) from the ZnSe as a result of two-photon absorption of the 800 nm light[33] was not observed due to the use of band-pass filters before detection. It should also be noted that SFG signals produced from the portion of the tip that is within the focal volumes of the lasers would produce a constant level background throughout the entire image as the laser-tip geometry is held constant throughout each scan for that purpose.

Acknowledgment. This work was supported by the Experimental Physical Chemistry Division of the National Science Foundation.

Note Added in Proof. Following acceptance of this manuscript, a related work on photon scanning tunneling sum-frequency microscopy appeared (Shen, Y.; Swiatkiewicz, J.; Winiarz, J.; Markowicz, P.; Prasad, P. N. *Appl. Phys. Lett.* **2000**, *77*, 2946). In this work, the fundamental of a Nd:YLF laser (1047 nm) and its second harmonic (523.5 nm) were summed together on prolinol nanocrystals. We reiterate, however, that our work constitutes the first demonstration of SFG NSOM, as well as the first example of scanning probe microscopy that utilizes an infrared source which, furthermore, is tunable.

LA001513M